ADVANCED ENERGY MATERIALS
www.advenergymat.de

Check for updates

# Materials-Related Strategies for Highly Efficient Triboelectric Energy Generators

*Yeon Sik Choi, Sang-Woo Kim,* and Sohini Kar-Narayan**

**Since 2012, triboelectric energy harvesting technologies have received a substantial amount of attention as they constitute one of the most efficient ways of transforming vibrational and frictional energy into electrical energy, regardless of location and environmental conditions. One of the most significant advantages of this technology is in the suitability of a very wide range of materials that can be readily incorporated into devices. In order to achieve efficient energy harvesting performance, advances in materials science and nanotechnology have been applied to develop high-performance triboelectric energy harvesters, which have witnessed a tremendous growth in popularity. However, even though a large number of materials, including polymers, metals, inorganic and composite materials, have been separately studied for triboelectric energy harvesting applications, the key features of these different classes of materials have never been presented together or summarized, to provide valuable insight for future materials development in this field. Here, a comprehensive review of the up-to-date materials-driven progress of triboelectric energy harvesting devices is provided, with emphasis on the study of materials-related operating mechanisms and emergent materials design strategies for highly efficient triboelectric devices. The discussion includes several issues and challenges that need to be addressed for further improvement of triboelectric devices.**

## 1. Introduction

The rapidly growing demand for energy solutions has prompted great interest toward environment-friendly energy harvesting devices. Recently scavenging mechanical energy from vibrations and frictional motion, such as human motion, rotating motion of machines, flowing water, and more, has attracted worldwide attention as these are easily available from ambient sources and applicable for portable and wearable electronic devices and wireless sensors. Piezoelectric and triboelectric devices are well-known energy harvesting methods which are able to transform such vibrational and friction energy into electrical energy. Although piezoelectric devices have been studied for a long time and commercialized for various applications, a limited number of applicable materials (e.g., materials with non-centrosymmetric crystal structure[1]) prevent the further improvement of output performance and extension of the range of applications. In contrast, triboelectric devices, such as triboelectric nanogenerators (TENGs), can easily incorporate different classes of materials, including metal, inorganic, polymer, and composite, as the working principle is based on ubiquitous static electricity.[2] (The term TENG refers to a device where nanomaterials or nanostructuring plays a role in the device performance. TENGs have widely been reported in the literature as large enhancements in performance can be achieved by this route. However, the topics covered in the review apply more broadly to devices where this is not necessarily the case but which can still be termed as triboelectric energy harvesters or devices.) In addition, outstanding power and energy conversion efficiencies of triboelectric devices enable them to be introduced to different applications, from sensors to energy generators.

In the early stages of this research field, the focus was on the structural design of triboelectric devices and their possible applications.[3–6] As a result, most of the performance enhancement reported originated from structural optimization, and the number of materials reported was generally limited to a few. It was not until recently that new and advanced materials and processing techniques have been suggested for triboelectric devices. However, most of the material-related research has been conducted without directionality, and the key features of materials related to device performance have rarely been collated. Therefore, a comprehensive review of the up-to-date materials-driven progress of triboelectric devices, with the study of the materials-related operating mechanism is essential to further enhance the energy harvesting efficiency and extend the range of applications.

Here, an overview of the fundamentals of triboelectric devices will be presented with material-related theoretical models compared to the classical device-related models. Then,

Dr. Y. S. Choi, Dr. S. Kar-Narayan
Department of Materials Science and Metallurgy
University of Cambridge
27 Charles Babbage Road, Cambridge CB3 0FS, UK
E-mail: sk568@cam.ac.uk
Prof. S.-W. Kim
School of Advanced Materials Science and Engineering
Sungkyunkwan University (SKKU)
2066 Seobu-ro, Suwon 16419, Republic of Korea
E-mail: kimsw1@skku.edu
The ORCID identification number(s) for the author(s) of this article can be found under https://doi.org/10.1002/aenm.202003802.

DOI: 10.1002/aenm.202003802

 © 2021 Wiley-VCH GmbH

several material-based strategies to improve the performance of these devices, and the future outlook of these materials will be discussed.

## 2. Fundamental Principle

### 2.1. Operating Mechanism

The key mechanisms of triboelectric energy harvesting are "contact electrification" and subsequent "electrostatic induction."[3,4] Contact between two different materials causes a charge transfer between the surfaces of the materials.[7–10] The material which gains charges becomes negatively charged, and the material which loses charges becomes positively charged; this phenomenon is known as "contact electrification."[11,12] Such charge transfer is attributed to electron,[13–17] ion,[18] and/or material[19] movement between two materials. The thermodynamic driver for charge transfer varies depending on the materials in contact. For example, when two metals with different work functions are brought into contact, charge transfer will occur until the chemical potential of the electrons (Fermi level) is the same everywhere.[20] For metal-dielectric (ceramic) contact, the local heating model suggests that the temperature-difference-induced charge transfer can be attributed to the thermionic-emission effect, in which the electrons are thermally excited and transfer from a hotter surface to a cooler one.[21] The trapped charge tunnelling model explains the size-dependent charging of a granular system of chemically identical insulators.[22] In the case of contact with soft materials, such as metal-polymer contact, the flexoelectricity model has been suggested and shows that the mechanical deformations by contacting or rubbing yield surface potential differences via flexoelectric coupling, thereby driving charge separation and transfer.[20] Other than the type of material involved, a number of factors, such as electron affinity, electronegativity, surface roughness, asperity size, and local topography, affect the so-called "charge affinity" (i.e., direction and magnitude of the surface potential differences). The charge affinity of materials is sometimes referred to as "triboelectricity," thus such charge transfer phenomena and the resulting transferred charges on the surface are called "triboelectric effect" (or triboelectrification) and "triboelectric charge," respectively. Since too many materials-related factors are intertwined, researchers have come up with an empirical arrangement of materials according to their ability to gain or lose charges when two materials are contacted, and this arrangement is called a "triboelectric series".[23] Typical triboelectric series includes common materials, and this table can be extended to all kinds of materials, including metal, ceramics, and polymers.[3,24] Materials located in the relative positive region, called tribo-positive materials, easily lose charges when they come in contact with other materials, and those on the relative negative region, called tribo-negative materials, tend to gain charges upon contact. Materials that are far apart with respect to their position in the series are thus desirable for greater charge transfer upon contact. When transferred charges (i.e., triboelectric charge) are generated on the surfaces of materials, such charges can be moved or stored within the materials even in the dielectric materials. In addition, the transferred charges can also be lost through a connected electrode or the surrounding atmosphere. Therefore, contact electrification can be further divided into three subprocesses: charge transfer, charge storage and charge loss.

In general, triboelectric devices consist of a pair of dielectric materials (or at least one insulator) and attached electrodes, and such electrodes are connected via an external circuit. When two materials are contacted, there is no electron flow in the external circuit because transferred charges with opposite polarities are fully balanced. As the two surfaces are separated, transferred charges on the top surfaces of both materials induce charges on their respective bottom electrodes; this phenomenon is called "electrostatic induction." The induced charges create an electrical potential between the two electrodes under open-circuit conditions. In short-circuit condition, the resulting electrical potential causes electron flow in the external circuit in order to attain equilibrium. A periodic voltage (or current) output can thus be generated across the materials as a result of periodic relative motion between the two.

### 2.2. Geometry of Triboelectric Devices

Regarding the geometry of triboelectric devices, four different modes have been introduced (**Figure 1**): the vertical contact-separation mode,[25] the lateral sliding mode,[26] the single-electrode mode,[27] and the free-standing mode.[28] Although each geometry shares the same fundamental energy harvesting mechanism, namely contact electrification and electrostatic induction as described above, they have different working parameters and energy harvesting efficiencies according to their structure.[4] As shown in Figure 1a, in the case of vertical contact-separation mode, two dielectric layers, with a thickness of $d_1$ and $d_2$ and dielectric constants of $\varepsilon_{r1}$ and $\varepsilon_{r2}$, respectively, are stacked face to face and connected by external loads. The distance between two contact surfaces is defined as $x(t)$ and modulated periodically by an external mechanical force. The $\sigma$ indicates the triboelectric charge density induced by contact electrification during the mechanical contact of two plates. During separation, the induced electric potential difference is defined as $V$. Variation of $V$ can be a driving force of electron transfer between two electrodes, and $Q$ indicates the amount of transferred charges. (Detailed equations will be discussed in Chapter 3.) In the case of lateral sliding mode (Figure 1b), the top layer moves laterally with lateral separation distance $x(t)$. At the fully overlapped position, $\sigma$ of the same magnitude but opposite signs are developed on both surfaces by contact electrification similar with the vertical contact-separation mode. When the top dielectric layer is sliding apart, the in-plane charge separation is initiated and induces a potential difference between top and bottom electrodes. This potential difference also drives a current flow, and developed current flow can be maintained with periodic relative sliding motion between the two surfaces. This means that the lateral sliding mode allows generation of energy from the surface of a rotational disk, which cannot be otherwise achieved by conventional piezoelectric- or electromagnetic-based devices.[29]

Figure 1c shows the schematic for the single-electrode mode. The starting position of the single-electrode mode is contact between the dielectric and the primary electrode, which causes


© 2021 Wiley-VCH GmbH

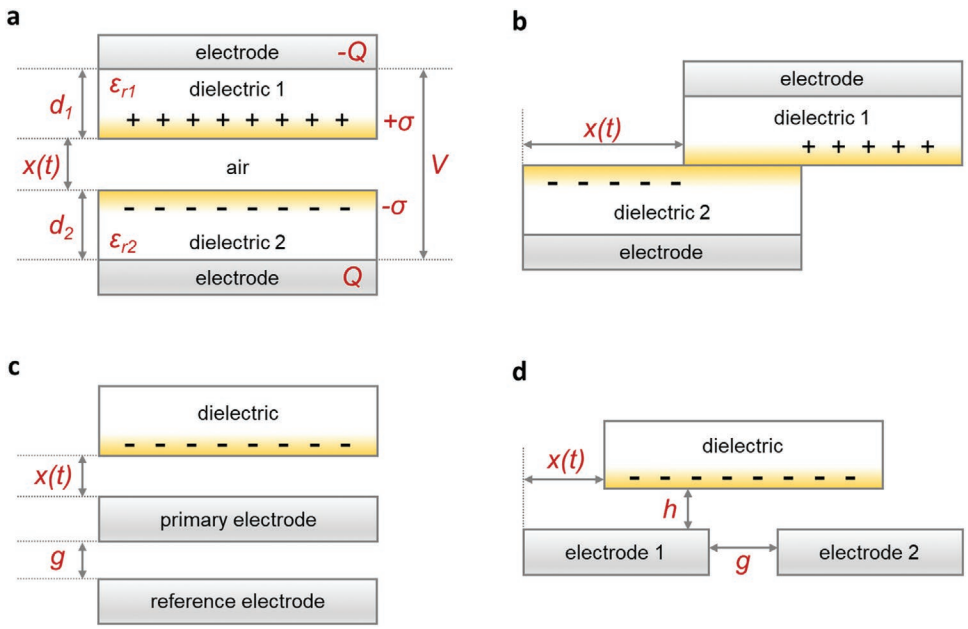


**Figure 1.** Four fundamental working modes of the triboelectric devices. a) The vertical contact-separation mode, b) the lateral sliding mode, c) the single-electrode mode, and d) the free-standing mode.

charge transfer from primary electrode to the dielectric layer with higher electron affinity. When the dielectric surface is separated from the primary electrode along the vertical direction, the amount of induced positive charge in the primary electrode increases as $x(t)$ increases. As a result, free electrons in the reference electrode flow to the primary electrode in order to balance the electric potential. During the motion, both electrodes are fixed, and a gap of $g$ is set to hold an identical geometric size. Although there is a loss of the charge transfer efficiency (i.e., the electrostatic screening effect),[27] the vertically aligned electrodes of single-electrode mode enables the free movement of the dielectric layer. As a result, this geometry has been applied to harvest energy from air[30] and from tyres,[31] and it was also applied as self-powered touch[32] and motion[33] sensors. In the case of free-standing mode (Figure 1d), two electrodes are placed in the same plane with a gap of $g$, and one freestanding dielectric layer is located above the electrodes with a vertical distance of $h$. When the dielectric layer is moved back and forth, triboelectric charge can be induced on both dielectric and electrodes surfaces, resulting in charge flows across the two electrodes. Due to the horizontally alignment of two electrodes, this mode does not have the electrostatic screening effect and enables high energy conversion efficiency.[34]

To develop triboelectric devices, therefore, device geometry should be carefully considered depending on target applications. In this review, all triboelectric devices are discussed based on the vertical contact-separation mode (Figure 1a) in order to focus on the influence of material itself on the device performance.

## 3. Theoretical Model

In order to predict the output behaviour of a triboelectric device, several theoretical models have been proposed, and they can be classified into two different categories: 1) device-related model and 2) material-related models. All device-related models assumed that an equal density of opposite triboelectric charges are uniformly distributed on the contact surfaces, and their densities are unchanged once the surfaces are charged. In other words, the triboelectric materials involved are considered as a perfect insulator. Whereas, in material-related models, it is assumed that triboelectric charges can move or be lost.

### 3.1. Device-Related Model

#### *3.1.1. Classical Model*

Researchers have developed a theoretical model based on a planar circuit element.[25–28] In the dielectric-to-dielectric contact-separation mode triboelectric devices, the electric field strength ($E$) of one dielectric part is derived by Gauss's law and given by

$$E = \frac{Q}{S\,\varepsilon_0\,\varepsilon_r} \tag{1}$$

where $Q$ is the value of the transferred charges between the two electrodes, $S$ the area of the electrode, $\varepsilon_0$ the permittivity of the vacuum ($8.854 \times 10^{-12}$ F m$^{-1}$), and $\varepsilon_r$ the relative permittivity (i.e., dielectric constant) of dielectric material.[25] The electric potential difference ($\Delta V$) between two electrodes can be thus given by

$$\begin{aligned}\Delta V &= E_1\,d_1 + E_2\,d_2 + E_{air}\,x(t)\\ &= \left[-\frac{Q}{S\,\varepsilon_0\,\varepsilon_{r1}}\,d_1\right] + \left[-\frac{Q}{S\,\varepsilon_0\,\varepsilon_{r2}}\,d_2\right] + \left[\frac{S\,\sigma - Q}{S\,\varepsilon_0}\,x(t)\right]\\ &= -\frac{Q}{S\,\varepsilon_0}\left(\frac{d_1}{\varepsilon_{r1}} + \frac{d_2}{\varepsilon_{r2}} + x(t)\right) + \frac{\sigma\,x(t)}{\varepsilon_0}\end{aligned} \tag{2}$$


© 2021 Wiley-VCH GmbH

where $d_1$ and $d_2$ are the thickness of the two dielectric materials, $x(t)$ the distance between two contact surfaces, t the time, $\sigma$ the triboelectric charge density, and $\varepsilon_{r1}$ and $\varepsilon_{r2}$ the dielectric constants of the two dielectric materials (in the conductor-to-dielectric structure, $t_1/\varepsilon_{r1}$ can be ignored because the metal layer acts as both triboelectric layer and electrode). Under open-circuit conditions, the value of transferred charge ($Q$) becomes zero since no charge is transferred between electrodes. Thus, if we assume the electric potential of the bottom electrode to be zero, the equation for the open-circuit voltage ($V_{oc}$) can be calculated to be

$$V_{oc} = \frac{\sigma}{\varepsilon_0} x(t) \tag{3}$$

From the experimentally determined $V_{oc}$ of each triboelectric device, the theoretical triboelectric charge density ($\sigma$) can be estimated by

$$\sigma = \frac{V_{oc}\,\varepsilon_0}{x(t)} \tag{4}$$

Under short-circuit conditions ($V$ = 0), the short-circuit transferred charge ($Q_{sc}$) is given by

$$Q_{sc} = \frac{S\,\sigma\,\varepsilon_{r1}\,\varepsilon_{r2}\,x(t)}{d_1\,\varepsilon_{r2} + d_2\,\varepsilon_{r1} + \varepsilon_{r1}\,\varepsilon_{r2}\,x(t)} \tag{5}$$

The value of $Q_{sc}$ can therefore vary as a function of $x$. In the case of conductor-to-dielectric structure, $Q_{sc}$ is given by

$$Q_{sc} = \frac{S\,\sigma\,x(t)}{d + x(t)} \tag{6}$$

Then, short-circuit current ($I_{sc} = \mathrm{d}Q_{sc}/\mathrm{d}t$) is given by

$$I_{sc} = \frac{S\,\sigma\,v(t)\,d}{\left(d + x(t)\right)^2} \tag{7}$$

Since we can measure the $I_{sc}$ from the device, the $Q_{sc}$ is also calculated using the integration of experimentally achieved $I_{sc}$.

Based on this classical model, a figure-of-merit (FOM) for triboelectric devices has been suggested,[35] as described in the following equation

$$\mathrm{FOM_s} = \frac{2\varepsilon_0}{\sigma^2}\,\frac{E_m}{S \cdot x_{max}} \tag{8}$$

where $\mathrm{FOM_s}$ is the dimensionless structural FOM, $E_m$ the largest possible output energy per cycle, and $x_{max}$ is the maximum displacement between two different materials.[35]

### 3.1.2. Distance-Dependent Electric Field Model

Although this classical model has been widely used to demonstrate the experimental results of triboelectric devices in the literature, it cannot clearly explain the mechanism of polarization of the dielectric layer and free-charge induction on the electrodes. This is because the classical model assumes that electric field perpendicular to a charged plane is uniform throughout the intervening space, and the magnitude of the electric field does not change with the distance from the charged surface.[36] Dharmasena et al. subsequently introduced an advanced theoretical model using the concept of a distance-dependent electric field.[36,37] To calculate the variation of electric field with distance, the $z$-axis electric field ($E_z$) above the midpoint (along with the $z$-axis) of a charged surface in free space is defined by Gauss's law. In the dielectric-to-dielectric contact-separation mode triboelectric devices, the electric field ($E$) at the dielectric-electrode interface is given by

$$E = \frac{\sigma}{\pi\,\varepsilon_{r1}}\left[f(d) - f(x+d)\right] \tag{9}$$

where

$$f(d) = \arctan\left(\frac{1}{2(d/L)\sqrt{4d^2/L^2+2}}\right) \tag{10}$$

Assuming that $L$ is the dimension of a square-shaped dielectric material, the $V_{oc}$ can be calculated by

$$V_{oc} = \frac{\sigma}{\pi\,\varepsilon_{r1}}\left[M(d)\right]_{d_1}^{d_1+x} + \frac{\sigma}{\pi\,\varepsilon_{r2}}\left[M(d)\right]_{d_2}^{d_2+x} \tag{11}$$

where

$$M(d) = x\arctan\left(\frac{L}{2d\sqrt{4d^2/L^2+2}}\right) - \frac{L}{w}\ln\left(\frac{1+\sqrt{4d^2/L^2+2}}{-1+\sqrt{4d^2/L^2+2}}\right) \tag{12}$$

Under short-circuit conditions ($V$ = 0), the short-circuit transferred charge ($Q_{sc}$) is given by

$$Q_{sc} = \frac{\sigma\,S\left[\frac{1}{\varepsilon_{r1}}\left[M(d)\right]_{d_1}^{d_1+x} + \frac{1}{\varepsilon_{r2}}\left[M(d)\right]_{d_2}^{d_2+x}\right]}{\left(\frac{1}{\varepsilon_{r1}} + \frac{1}{\varepsilon_{r2}}\right)\left[M(d)\right]_0^{d_1+d_2+x}} \tag{13}$$

Consideration of the electric field variation with the distance results in the non-zero overall electric field, which depends on the separation distance, and this enabled the explanation of dielectric polarization and electron rearrangement.

### 3.1.3. The Resistance–Capacitance Product Matching Model

From a practical point of view, a different FOM for maximum power density was also presented by Peng et al.[38] They pointed out that the periodic mechanical motion of contact-separation mode triboelectric devices changes the distance ($x$) between two dielectric surfaces and results in the time-varying capacitance of dielectric layer and air gap. Furthermore, they argued that, to achieve the most effective generator with maximum power density, the mechanical motion with constant frequency ($\omega$) should be matched with the characteristic frequency of the circuit ($1/\mathrm{RC_{total}}$). By matching the resistance–capacitance (RC)


© 2021 Wiley-VCH GmbH

product to $\omega$, the device FOM ($FOM_{device}$) for the maximum power density is defined by

$$FOM_{device} = 0.064 \cdot \frac{\sigma^2 \cdot \bar{v}}{\varepsilon_0} \tag{14}$$

where $\bar{v}\,(=\omega x_{max}/\pi)$ is the average speed of the mechanical motion. It shows that $\sigma$ is the only material-related parameter that needs to be considered for the maximum power density.

### 3.2. Material-Related model

#### 3.2.1. Dynamic Charge Model

According to the Equations (5) and (13), the triboelectric charge density, which is the density of transferred charges on the surface, is the only materials-related parameter for triboelectric performance. This means that charge transfer is the only critical process that needs to be considered for a highly efficient device. However, it must be noted that such device-related models assume that triboelectric charges are placed only on the top surface of the dielectric material and do not move or dissipate (**Figure 2**a). As a result, these conventional models are also called "static charge models." Considering the motion of triboelectric charges in the dielectric layer, it is obvious that the charge storage and loss process should also be considered. Cui et al. have suggested a "dynamic charge model" to elucidate the motion of charge in the dielectric layer.[39] Given that the movement of charge is determined by the properties of the material, this model would be classified as a "material-related model."

As shown in Figure 2b, the dynamic charge model assumes that triboelectric charge can be moved and stored (or lost) in the dielectric layer by two different mechanisms: an electric field-induced drift, and recombination with the charge on the electrode, respectively. In order to simplify the model, diffusion caused by the concentration gradient, an impact of trap level, and the absorbance of charge from the atmosphere were ignored. In addition, a large electric field ($E$) and a much larger surface area than thickness were also assumed. As a result, triboelectric charges are distributed within the whole dielectric layer (Figure 2c). In addition, the quantity of triboelectric charge ($q$) can vary with the thickness of the dielectric layer due to the loss process (Figure 2d). In static charge models, the value of $q$ is constant regardless of the thickness of the dielectric layer because it is assumed that $q$ is determined by contact electrification and is not altered. In contrast, in the case of the dynamic model, $q$ increases with dielectric layer thickness because charge can be lost easily in thin dielectric materials. If the dielectric layer is expressed as discrete $n$ sublayers in a direction parallel to the surface, space and time-dependent electric field ($E_{x,t}$) of each layer is defined by

$$E_{x,t} = \frac{\sum_0^i q_{(i,t)}}{\varepsilon_0\, \varepsilon_r\, S} \tag{15}$$

where $q(i,t)$ is the triboelectric charge quantity, $i$ the number of sublayer, and $S$ the surface area of the dielectric layer. Then, the Gaussian probability density function for the drift distance of charge is given by

$$f\,(i,t) = \frac{1}{\sigma\sqrt{2\pi}}\, e^{-\frac{1}{2}\left(\frac{x-\mu\, E_{i,t}}{\sigma}\right)^2} \tag{16}$$

where $\mu$ is the electron mobility in the dielectric materials, and $\sigma$ the standard deviation. The quantity of triboelectric charge carried in $i$ th sublayer can be described as

$$q_{(i,t+\Delta t)} = \sum_0^i \left[q_{(i-1,t)} \cdot f\,(i,t)\right] - q_{(i,t)} \int_{i\Delta x}^{n\Delta x} f\,(i,t) \tag{17}$$

where $\Delta x$ is the thickness of each sublayer. The electron drift modelling confirms that a large amount of triboelectric charge becomes lost in the thin dielectric layer. When the thickness of dielectric layer increases, the total amount of triboelectric charge increases and is saturated at certain value of thickness, as triboelectric charge cannot reach the dielectric/electrode interface due to the induced electric field in the thick dielectric film (Figure 2d, orange).

This dynamic charge model gives interesting insight regarding the output performance of triboelectric devices. Typically, researchers predicted that much more short-circuit transferred charge ($Q_{sc}$) could be achieved from a triboelectric device with a thinner dielectric layer based on the conventional static charge model. According to the Equations (5) and (7), $Q_{sc}$ and $I_{sc}$ are inversely proportional to the thickness of the dielectric layer in the contact-separation mode triboelectric devices (Figure 2e). However, if triboelectric charges are moved and lost by combining with induced charges at the dielectric/electrode interface, the triboelectric charge density ($\sigma$) could decrease easily in the hin dielectric layer. In other words, when the dielectric layer is thin, triboelectric charge with drift mobility ($\mu$) can easily be moved and combined with charge in the electrode by electric field, resulting in a low output of $Q_{sc}$ at the equilibrium condition. It means that calculation of output performance based on conventional static charge model cannot be applied for a triboelectric device with a thin dielectric layer. When the dielectric is thick enough, the relationship between $Q_{sc}$ and thickness is similar to the static charge model because the $\sigma$ can be preserved during the motion.[40] These results indicate that there is an optimum thickness for the maximum $Q_{sc}$ (Figure 2f). Considering that $\mu$ is the material-related parameter, the dynamic charge model implies that the triboelectric charge storage and loss mechanism can also be controlled through material processing.

## 4. Strategies to Improve Triboelectric Performance of Materials

To realise an efficient triboelectric device, the majority of research to date has focused on finding the best pair of materials as this is critical to efficient charge transfer. Versions of the triboelectric series have been used to select appropriate pairs of materials because it is known that materials that are further apart in the series result in a greater relative charge transfer.


© 2021 Wiley-VCH GmbH

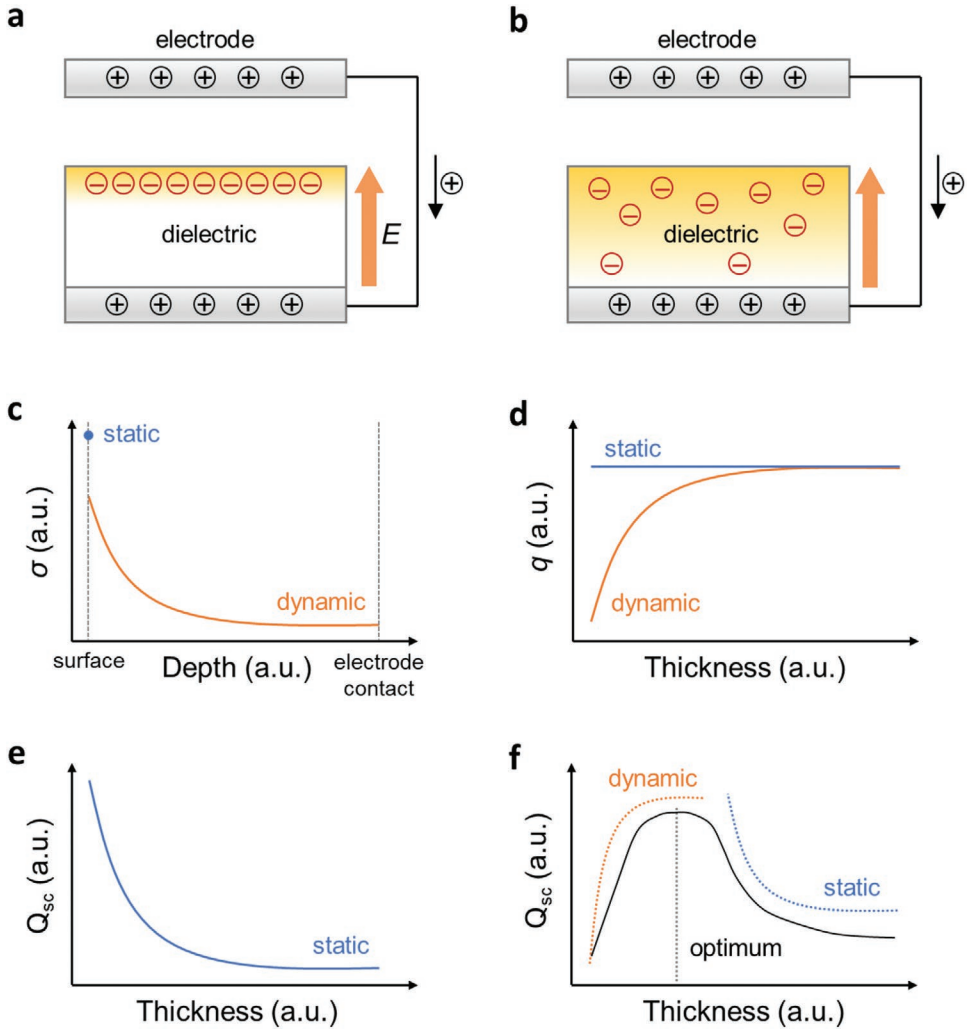


**Figure 2.** Schematics of the contact-separation mode triboelectric devices with two different assumptions: a) conventional static charge model and b) dynamic charge model. Red and blue circles indicate transferred electron by contact electrification and induced positive charge, respectively. c) Theoretical triboelectric charge distribution in the dielectric layer of (blue) static and (orange) dynamic charge model. d) Theoretical relationship between the quantity of triboelectric charge ($q$) and thickness of the dielectric layer. e,f) Theoretical relationship between short-circuit transferred charge ($Q_{sc}$) and thickness based on e) static charge model and f) dynamic and static charge model.

Thus, triboelectric devices based on pairs of materials located on the extreme opposite ends of the triboelectric series are expected to show superior energy harvesting capabilities. For example, the combination of fluorinated polymers and metals have been the most commonly used materials in triboelectric device-related research to date. However, purely triboelectric series-based material selection has shown limited performance enhancement. In addition, this would not be a reliable approach because, as we aforementioned, such tables are empirically arranged. The second major approach is through structural modification to increase the contact surface area, as seen in a lot of triboelectric device-related research. Based on the contact-separation mode, multilayered and stacked triboelectric devices have been suggested in order to enhance the total output power,[41,42] but the accompanying bulky volumetric structure and limited possible applications constitute challenges to this approach. Forming nanostructures, such as nanowires or nanotubes, or patterns of pyramid-, square-, or hemisphere-based micro- or nanopatterns have also been shown to improve the power output performance of triboelectric devices.[43–49] However, these rough structures get damaged physically in the long-term due to continuous contact between surfaces, causing a reduction in energy conversion efficiency. As a result, lifetimes of such nano- and micro-structured polymer surfaces severely affect the reliability of the device performance. Above all, these surface-area-related approaches offer limited performance enhancement since only an increase in surface area for contact is achieved, but the inherent energy harvesting capabilities of the material remains unchanged.

Recently, material-related performance enhancement approaches have been proposed. By introducing functional materials or by functionalizing the material itself, further improvement of device performance can be achieved. The methods for improvement of triboelectric performance are divided into two parts based on the property manipulating mechanism: charge generation and charge storage. **Figure 3**

 © 2021 Wiley-VCH GmbH

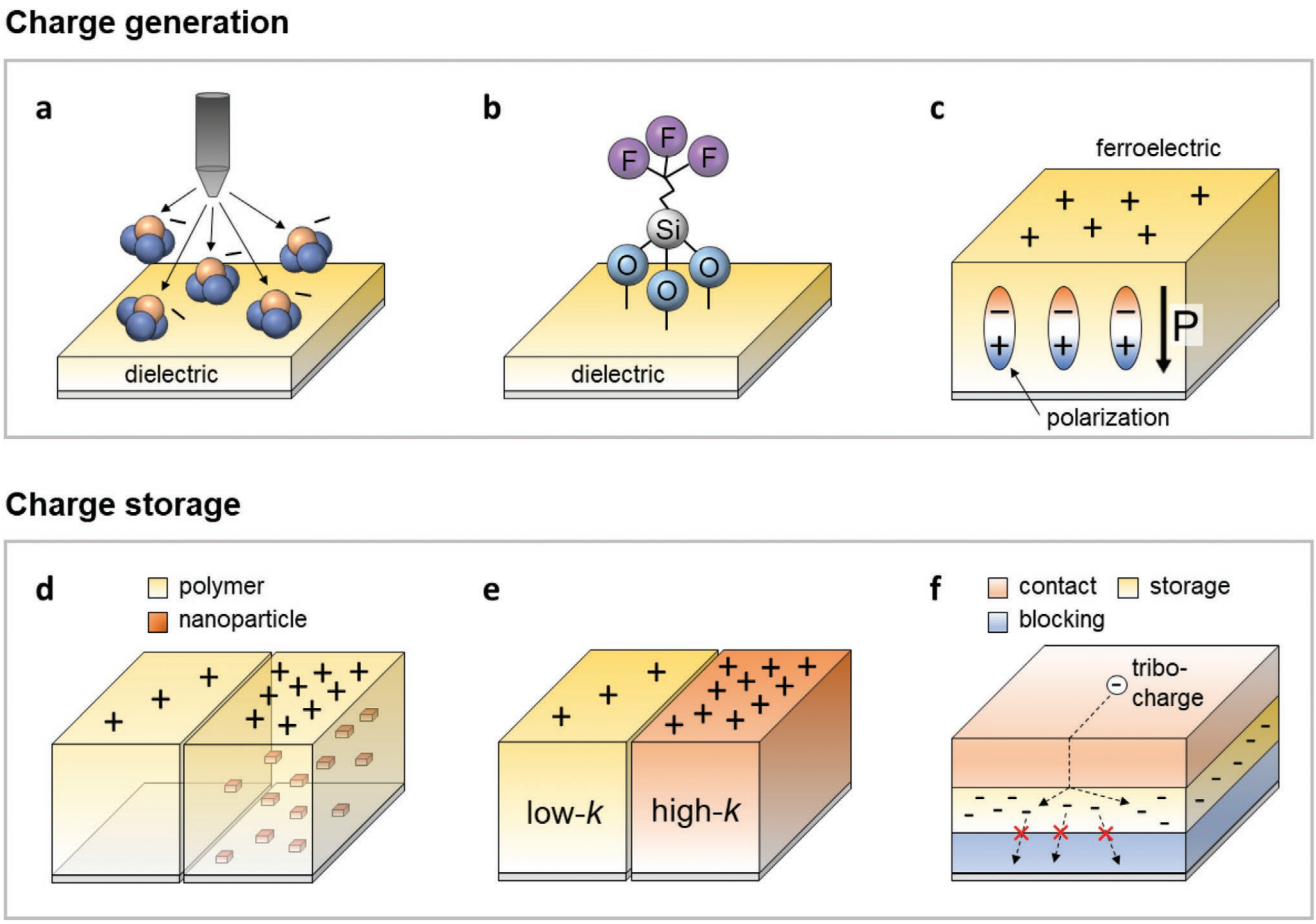


**Figure 3.** Various strategies to improve the performance of triboelectric devices: a–c) charge generation and d–f) charge storage methods. a) Charge injection into the dielectric layer by the corona discharging. Grey schematic indicates the air-ionization gun. Possible generated charged molecules are $CO_3^-$, $O_3^-$, and $NO_3^-$. b) Surface chemical functionalization of the dielectric layer. Schematic illustrates a generated self-assembled monolayer (SAM) on the dielectric material. c) Realization of spontaneous polarization in ferroelectric materials. d) Polymer-based nanocomposite for enhanced charge storage capabilities: polymer layer without nanoparticles (left), and with nanoparticles (right). The yellow area and orange cube indicate polymer matrix and inorganic nanoparticles, respectively. e) High dielectric constant (high-*k*) material for enhanced triboelectric charge density. f) Formation of the multi-layered structures. The dotted line shows the movement of the triboelectric charge. Red, yellow, blue layers indicate contact, charge storage (or trap), and charge blocking layers, respectively. Each layer can be selected and assembled for the best charge storage performance.

displays the schematics of each method. Here, we would like to classify the charge generation method intro three categories: ion injection, surface functionalization, and surface polarization.

### 4.1. Charge Generation

By transferring charge during contact, triboelectric charges are placed on the surface of a material, and the resulting triboelectric charge density is one of the critical material-related factors which affects the output of triboelectric devices. Therefore, an additional generation of triboelectric charge or increasing surface charge density is an effective approach to improve device performance. To be clear, both "triboelectric charge density" and "surface charge density" should be defined separately. Triboelectric charge density should be limited to transferred charge on the surface by contact electrification. In contrast, surface charge density can be defined as density of the total charge on the surface regardless of origin. The density of surface charge can be measured using Kelvin probe force microscopy (KPFM).

#### *4.1.1. Ion Injection*

By injecting single-polarity charged particles/ions via air-ionization gun or corona discharging on grounded dielectric layers, surface charge density has been shown to be directly modulated (Figure 3a).[50] The surface charge density increased with a number of injections and reached a maximum level due to air breakdown (**Figure 4**a). At the maximum surface charge density ($\sigma_{max}$), 25-fold enhancement of triboelectric output performance was achieved by ion-injection method. Although this charge injection method is one of the facile ways to improve the device performance, there are some critical issues related to the triboelectric charge storage. First of all, ion-injection method can only be introduced to device with a relatively thick dielectric layer with low charge loss due to the limited charge storage

 © 2021 Wiley-VCH GmbH

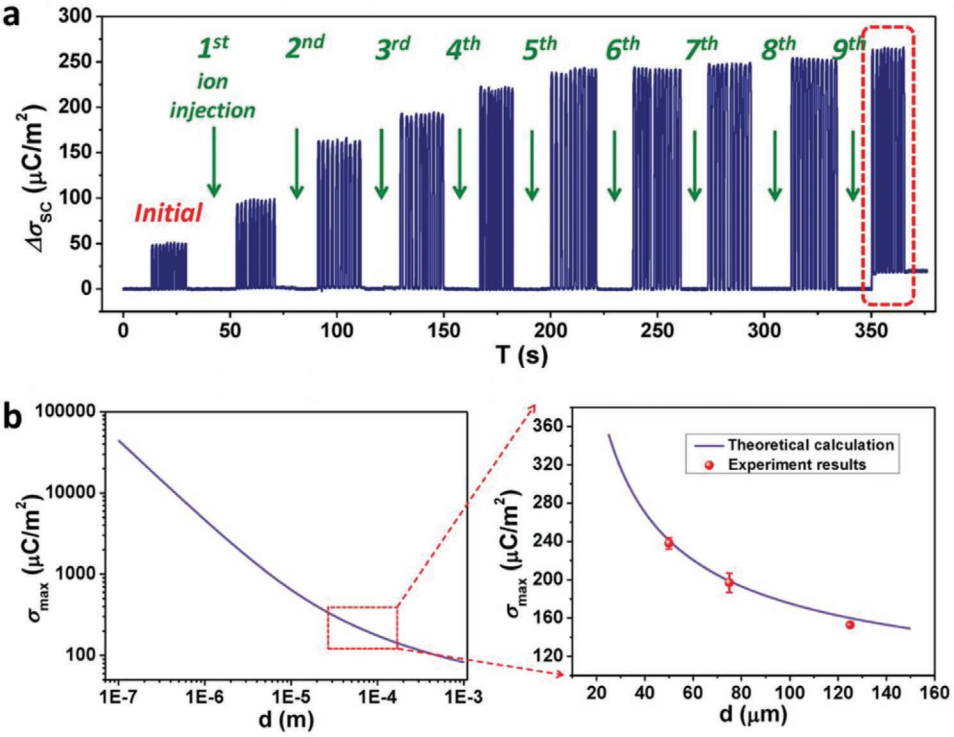


**Figure 4.** a) Step-by-step measurement of the ion-injection process and study of the maximum surface charge density for the triboelectric devices. Elevation of the short-circuit charge density ($\Delta\sigma_{SC}$) generated by the triboelectric generator when the FEP film was injected with ions time by time. b) Theoretical relationship between the maximum surface charge density ($\sigma_{max}$) and the thickness ($d$) of the FEP film. (right) Plot of the above theoretical relationship in the range of 20–150 µm, with the three points of the experimentally obtained $\sigma$ max for the $d$ of 50, 75, and 125 µm, respectively. Reproduced with permission.[50] Copyright 2014, Wiley-VCH.

capability. The relationship between $\sigma_{max}$ and the thickness of the dielectric film was also investigated by comparing the threshold voltage for the air breakdown and the actual voltage drop across the air gap in the triboelectric devices (Figure 4b). The theoretical and experimental research revealed that a larger $\sigma_{max}$ could be achieved in a thinner film. By reducing the thickness of fluorinated ethylene propylene (FEP) dielectric layer to the range of hundreds of nanometers, the surface charge density could be enhanced by a factor of two, with the 4-fold improvement of output power. However, the thinner dielectric layer indicates a higher possibility of electric loss, indicating there is a limited charge storage capability. It must be noted that the $\sigma_{max}$-thickness relationship and $Q_{sc}$-thickness relationship in Figure 2 are different. This is because the main consideration of ion injection is charge storage capability in dielectric layer and the air-breakdown. In contrast, the $Q_{sc}$ relationship assumes the same triboelectric charge density and focuses on the possibility of charge loss. Secondly, although the thick dielectric material is used, the triboelectric charge density is slowly attenuated due to water vapour and charged particles that exist in air. The density of the injected surface charge on the thick FEP layer was reduced ≈16.6% over 20 days. It means that triboelectric materials are not appropriate for some application, such as vibration monitoring and low-frequency active sensors,[51] which needs to work for only a few seconds at a time and then remain for hours or more. The charge loss rate was also found to vary depending on the type of materials. Despite the same quantity of charge (≈240 µC m$^{-2}$) initially injected, more than 80% of surface charge density was lost in a Kapton film within 5 days, indicating that the charge storage (or loss) efficiency varies with material properties. Lastly, as briefly stated above, due to the air breakdown, the amount of storage charge is restricted regardless of the material used. Although high vacuum method,[52] self-improving device structure[51] and external charge pumping device[53] were suggested to resolve air-breakdown issue, high vacuum environment and huge device-size, due to the additional charge pumping components, make them difficult to be deployed in practical applications.

#### 4.1.2. Surface Functionalization

Triboelectric charge density can also be manipulated by modification of surface chemical structure. To functionalize the surface of a dielectric material, self-assembled monolayers (SAMs) have been introduced via dip-coating or vapour deposition method (Figure 3b). Poly-L-lysine and trichloro(1*H*,1*H*,2*H*,2*H*-perfluorooctyl) silane (FOTS) coated polyethylene terephthalate (PET) film resulted in positively and negatively charged surfaces, respectively.[54] 3-aminopropyltriethoxysilane (APTES), 3-glyci-doxypropyltriethoxysilane (GPTES), FOTS, and trichloro (3,3,3-trifluoropropyl) silane (TFPS) were also applied onto polydimethylsiloxane (PDMS) layer for negative (APTES, GPTES) and positive (FOTS, TFPS) surface potentials.[55] With


© 2021 Wiley-VCH GmbH

more sophisticated characterization, Shin et al. produced functionalized PETs with ten different surface potentials using halogen-terminated aryl-silane derivatives and aminated materials.[56] To be more specific, the surface potential of the dielectric layer was manipulated by functionalization processes with highly polarized functional groups, such as −F, −Cl, $-NH_2$, and amide groups. As a result, the tendency of electrostatic potential is consistent with the sequence of electron affinity of halogen atoms in the gas phase (Cl > F > Br), indicating successful modification of charge affinity (triboelectricity) of the polymer surface (**Figure 5**a). Furthermore, the surface modification enables enhancement of the triboelectric charge density on the contact surface and improvement of output performance in triboelectric devices. It means that the parameters related to charge affinities of surface molecules, such as electronegativity or electron density, is one of the key factors for the charge transfer process. As all other variables related to the property of the dielectric layer, including capacitance, mechanical stiffness and roughness, are fixed in surface functionalization studies, resulting trends give important evidence for the arrangement of a triboelectric series. In other words, it is possible to explain why the materials with negative functional groups (−F), such as fluorinated polymers, are located on the negative edge, but the materials containing positive groups ($-NH_2$, and amide group), such as Nylon, are placed on the positive region in the triboelectric series. Therefore, it is also possible to combine two different factors, which affect the charge transfer process, to further enhance the output performance. For instance, recent investigations states that the device performance can be improved more by combining both surface functionalization and morphological tuning related to charge affinity and surface area, respectively.[57,58] Despite the outstanding efficiency of surface modification methods, the durability of SAMs is a critical limitation because monolayered functionalized molecules are vulnerable to the frictional motion. To solve this issue, Yu et al. went further and engineered the properties of the bulk of the material, rather than just its surface.[59] By using sequential infiltration synthesis, they infiltrated $AlO_x$ molecules into polymer films and tuned the electrical properties of the polymer. The $AlO_x$ species inside the polymer film allowed the creation of high-performance triboelectric devices. In addition, due to the diffusion depth of ≈3 µm, the resulting enhancement was found not to have been diminished even after the polymer surface was worn out during long-term operation. Ryu et al. suggested solid polymer electrolyte-based triboelectric devices.[60] The addition of various ions successfully changed the surface potential of polyvinyl alcohol (PVA) electrolyte, improving triboelectric output performance with high durability (more than 30 000 cycles) (Figure 5b). The enhanced output of solid polymer electrolyte can be explained using the work function model. Typically, insulators have large band gaps, which contain partially localized electron trap states between the lowest unoccupied molecular orbital and highest occupied molecular orbital. Also, electron charged states at relatively higher energy levels than electron unoccupied states mainly contribute to electron transfer in contact electrification between insulators. Therefore, the additional energy bands due to anions which have electron charged states or due to cations which have electron unoccupied states, affect ionic doping in PVA. For example, $CaCl_2$ electrolyte which has more anions,

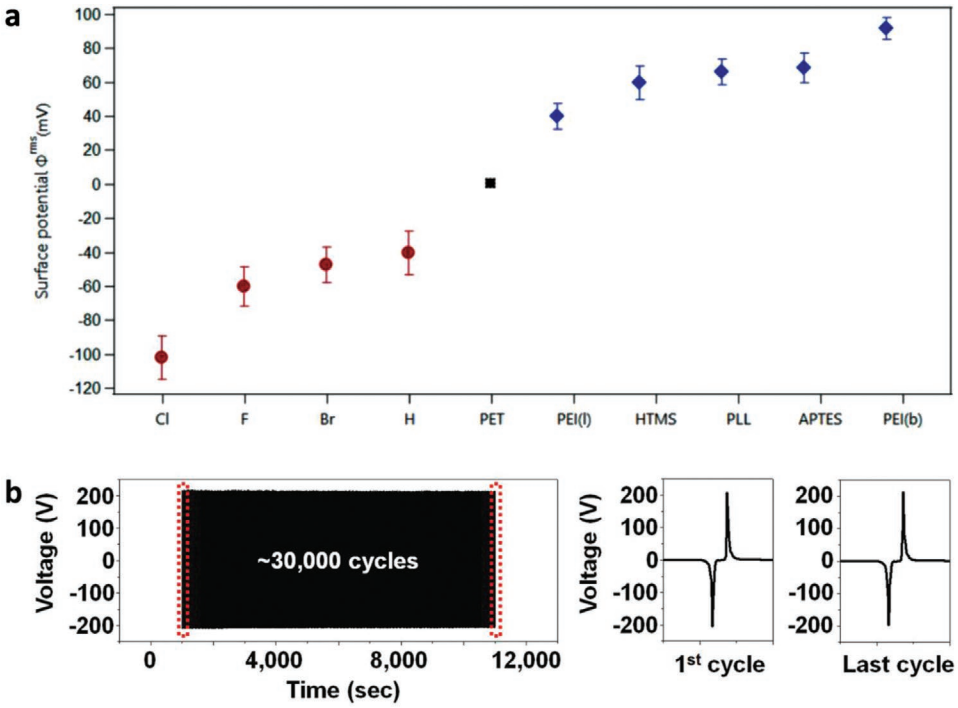


**Figure 5.** a) Electrostatic surface potentials (Φ) of functionalized PET surfaces, measured using KPFM. b) Durability test result of $CaCl_2$-PVA 0.75 M SPE-based triboelectric devices. Right graphs show the magnified voltage output for the first and last cycles. Reproduced with permission.[56,60] Copyright 2017, ACS, Wiley-VCH.


© 2021 Wiley-VCH GmbH

creates high-energy electron charged states in PVA, so that the additional electron charged states enhance the charge transfer potential of the base material in a contact electrification process.[60]

#### 4.1.3. Spontaneous Polarization

Spontaneous polarization (or remanent polarization) is the polarization which remains in a ferroelectric polymer when an applied electric field is reduced to zero.[61] Recent investigations have proposed that this spontaneous polarization can enhance triboelectric charge density (Figure 3c). Bai et al. demonstrated the substantial enhancement of the output power density of triboelectric devices using electrically polarized polyvinylidene fluoride (PVDF).[62] Lee et al. showed evidence of the changes in surface potential of polyvinylidene fluoride-trifluoroethylene (P(VDF-TrFE)) depending on the polarization direction.[63] When a P(VDF-TrFE) film was poled negatively, films acted as a tribo-positive material. In contrast, the positively poled film showed tribo-negative properties, increasing the output voltage compared to an unpoled film. These results indicate that the spontaneous polarization of the ferroelectric polymer can alter the triboelectric charge density as well as device performance. Based on piezo-response force microscopy (PFM) and KPFM analysis, the effect of spontaneous polarization on the triboelectric charge density has been demonstrated in more detail.[64] When P(VDF-TrFE) films were poled by an atomic force microscope (AFM) tip with different magnitude and direction of electric field, the KPFM measurement after the "rubbing" process due to the tip scanning across the sample surface (which imitates the frictional motion of a triboelectric device), showed that the spontaneous polarization further enhanced the amount of surface charge. This is possibly due to the modulation of work function between the ferroelectric polymer and contact material.[65] In more detail, the electrical poling caused the polarization-induced Fermi level shift in ferroelectric polymer and led to transfer of more charge from the metal counterpart to the ferroelectric polymer surface.

More recently, Choi et al. demonstrated "self-poled" ferroelectric nanowires that were fabricated without any external electrical poling process.[66–69] As a ferroelectric material, odd-numbered Nylon was investigated, which incidentally belongs to the less-explored family of synthetic and organic tribo-positive materials. They shows that $\alpha$-phase Nylon-11, which is the phase associated with strong hydrogen bonding, resulted in enhanced triboelectric charge density (**Figure 6**ai).[66] Thermally assisted nano-template infiltration (TANI) method was used to fabricate $\alpha$-phase Nylon-11 nanowires (Figure 6aii) which showed much higher surface potential and thermal stability compared to films or even $\delta'$-phase Nylon-11 nanowires with weaker hydrogen bonding. The higher surface potential was as a result of the nanoconfinement-induced self-polarization while the strong-hydrogen bonded crystal structure contributed to the enhanced thermal stability of $\alpha$-phase Nylon-11 nanowires (Figure 6b). Measurement of changes in surface potential by KPFM before and after mechanical rubbing using an AFM tip also verified the enhanced charge accumulation capability resulting from a higher net dipole moment of $\alpha$-phase nanowires (Figure 6c). As a result, the observed output power from $\alpha$-phase Nylon-11 nanowire-based triboelectric generator was shown to be ≈3 times and ≈34 times higher than those of $\delta'$-phase Nylon-11 nanowires and Al-based device used for comparison, respectively (Figure 6d).[66]

Separately, Busolo et al. suggested a way to control the surface potential of electrospun, "non-ferroelectric" polymer fibers, by controlling the polarity of the applied voltage during the fibre fabrication process.[70] The surface polarity of the electrospun poly(methyl methacrylate) (PMMA) was modified from positive to negative and vice versa by voltage driven molecular reorientation of the oxygen containing group. As a result, modified PMMA showed much higher surface potential and output performance than spin-coated PMMA. The great advantage of this spontaneous polarization approach is the durability of the device. This is because such spontaneous polarization is induced by the modification of the "internal" molecular structure of the materials, while ion injection and surface modification manipulate the molecules on the "surface" of dielectric materials. As a result, despite the abrasion of surface during periodic contact motion, materials with spontaneous polarization can maintain their output performance.

### 4.2. Charge Storage

During the contact and separation motion of a triboelectric device, the triboelectric charges in the dielectric layers induce the flow of free charges in an external circuit. However, as discussed, triboelectric charge can be dissipated, and this loss process is determined by the properties of the dielectric material. Here, we will classify the ways to reduce the loss of triboelectric charges into two categories: controlling the dielectric constant, and using a charge trap.

#### 4.2.1. Dielectric Constant

It has been argued that an increase in the dielectric constant of a material (i.e., relative permittivity) can enhance the triboelectric charge density ($\sigma$).[71,72] This is because the dielectric layer of a triboelectric device is modelled as part of a capacitor, and the capacitance ($C$) is defined as

$$C = \frac{\varepsilon_0 \, \varepsilon_r \, S}{d} \tag{18}$$

where $\varepsilon_r$ is the dielectric constant of the dielectric layer, $S$ the surface area, and $d$ the thickness of the dielectric layer. In this respect, polymer-based nanocomposites have been proposed to improve the dielectric constant with resulting enhanced output performance of TENGs (Figure 3d). For example, it was found that the 3-fold increase in $V_{oc}$ can be obtained by embedding barium titanate ($BaTiO_3$) nanoparticles into a PDMS dielectric layer, as compared to pure PDMS-based TENGs.[73] In addition, it could be clearly seen that the output performance of the TENG increased with increasing volume ratio of $BaTiO_3$ nanoparticles. Based on Maxwell model, the $\varepsilon_r$ of composite ($\varepsilon_{r,\,\text{composite}}$) is given by


© 2021 Wiley-VCH GmbH

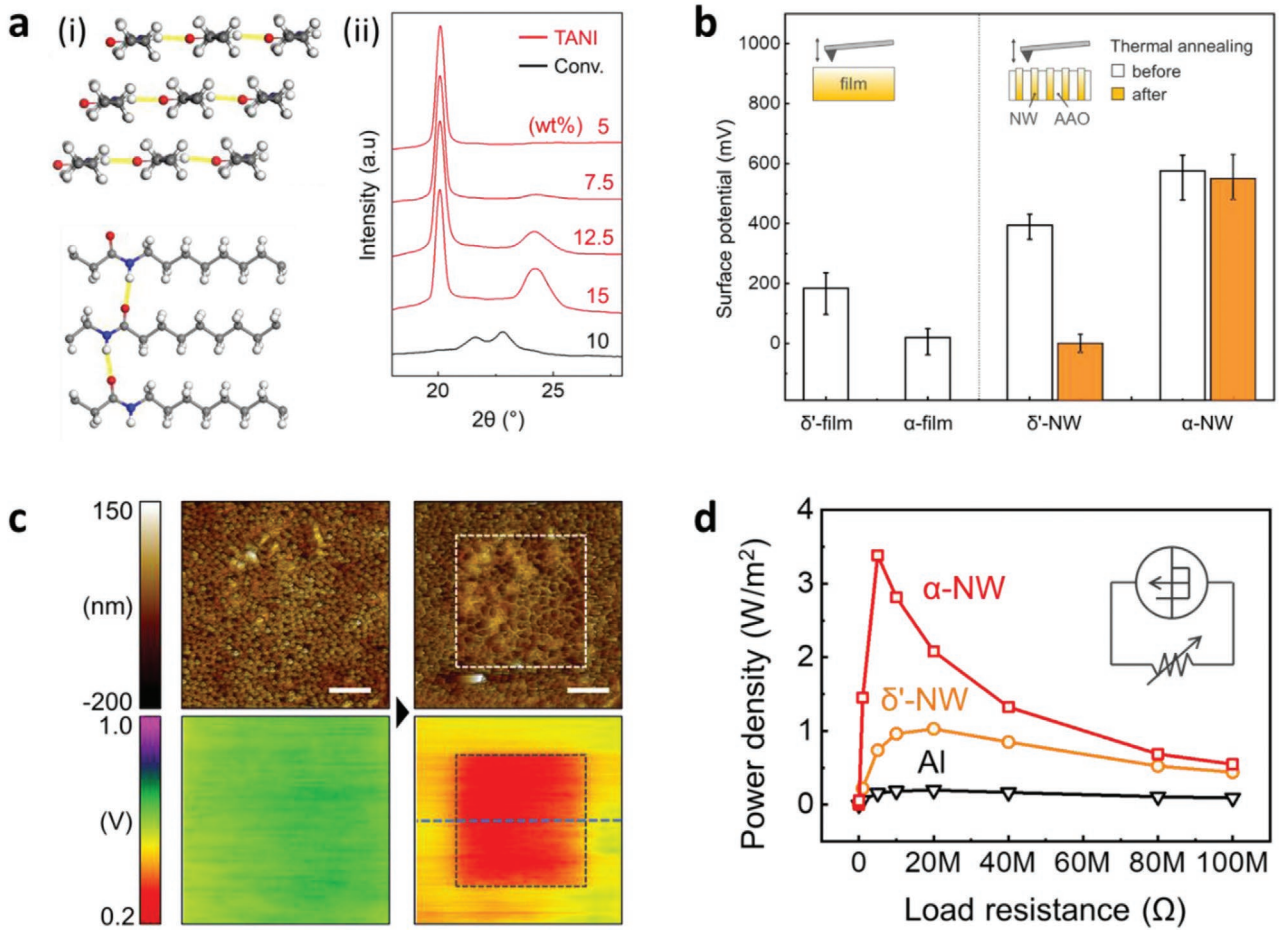


**Figure 6.** a) i) Molecular structure and chain packing of $\alpha$-phase Nylon-11. The fully stretched molecules in trans-configuration with sheets of strong hydrogen bonding generate a well-ordered structure. The yellow lines indicate intermolecular hydrogen bonding. ii) X-ray diffraction patterns of nanowires fabricated by the conventional template-wetting (black) and the TANI (red) methods. The XRD pattern of nanowires fabricated by TANI method with 5 wt% solution corresponds to that of $\alpha$-phase Nylon-11. b) The surface potential of various films and nanowires before (white bar) and after (orange bar) thermal annealing at 165 °C. c) AFM topology (top) and surface potential (bottom) changes in $\alpha$-phase nanowires before (left) and after (right) rubbing process. d) The power density of triboelectric generators with different combinations of materials. Reproduced with permission.[66] Copyright 2020, AAAS.

$$\varepsilon_{r,\text{composite}} = \varepsilon_{r,\text{ polymer}}\left[1+3\varphi_f\Big/\left(\frac{\frac{\varepsilon_{r,\text{ NPs}}}{\varepsilon_{r,\text{ polymer}}}+2}{\frac{\varepsilon_{r,\text{ NPs}}}{\varepsilon_{r,\text{ polymer}}}-2}-\varphi_f\right)\right] \tag{19}$$

where $\varepsilon_{r,\text{ polymer}}$ is the relative permittivity (i.e., dielectric constant) of the polymer matrix, $\phi_f$ the volume fraction of nanoparticles, and $\varepsilon_{r,\text{ NPs}}$ the relative permittivity of nanoparticles. This indicates that the relative permittivity increases with the increase of volume ratio of nanoparticles. The same effect of high dielectric constant (high-$k$) nanocomposite on device performance has been confirmed through studies of TENGs with Ag-exchanged zeolite[74] and graphite particle-based nanocomposite.[75] (The ways to control the dielectric constant of polymers by adding micro- or nano-sized materials are well-established in the field of nanocomposite, and have been extensively reviewed in the literature.[76,77] Therefore, we opted not to deal with it in more detail in this section.) To further enhance the performance of TENGs, nanoparticles have been introduced into mesoporous dielectric layers. By mixing PDMS with Au/water solution, a mesoporous structure was achieved after subsequent evaporation of the water. This Au nanoparticle-embedded mesoporous film-based TENG showed 5-fold power enhancement compared to a flat film-based device.[78] This is because the pores forming in the dielectric layer effectively reduce the thickness, while preventing electric shorting between top and bottom electrodes (**Figure 7**).[79] As a result, the capacitance could be improved by both high-$k$ nanoparticles and decreased thickness (by mesoporous structure). Furthermore, pores in the dielectric layer enlarged the surface contact area during contact electrification, increasing triboelectric charge density. This is the reason why a synergetic effect could be achieved by nanoparticles and pores, despite the air ($\varepsilon_r = 1$) in the pores reducing the total dielectric constant of the nanocomposite ($\varepsilon_{r,\text{ composite}}$). A triboelectric device with a high-$k$ polymer dielectric was proposed by Lee et al (Figure 3e).[71] Instead of adding inorganic nanoparticles, the $\varepsilon_r$ of PVDF layer was


© 2021 Wiley-VCH GmbH

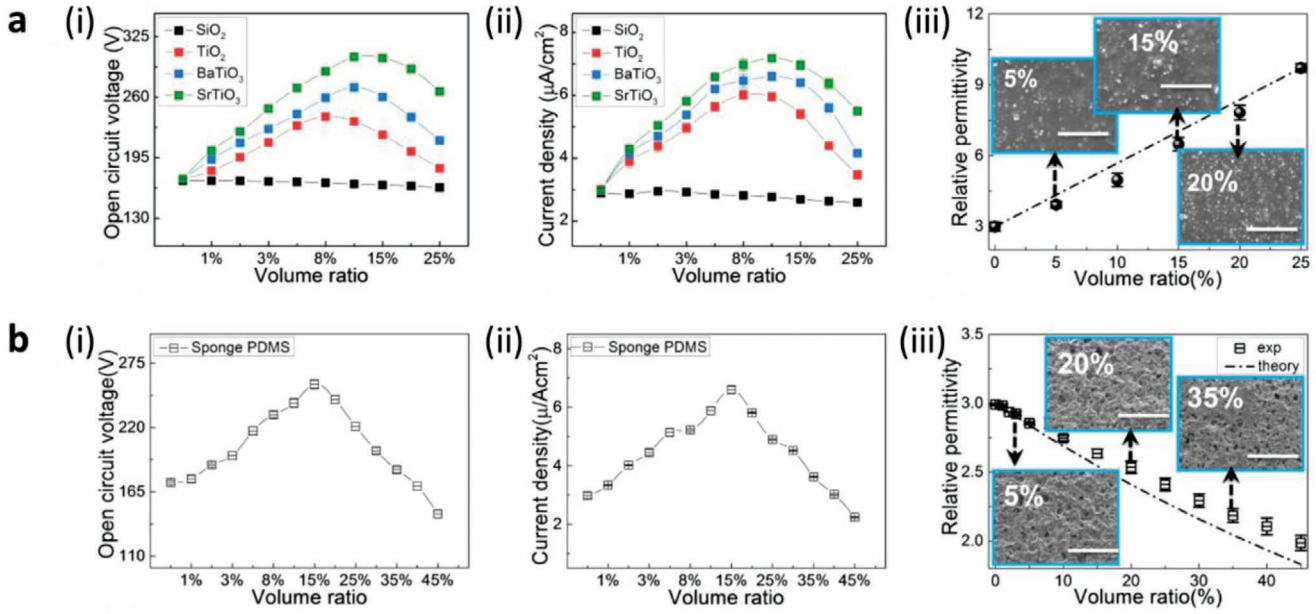


**Figure 7.** a) i) Open-circuit voltage and ii) short-circuit current density of the nanoparticle-filled samples with various volume ratios. iii) Relative permittivity changes as a function of $SrTiO_3$ content. The insets show SEM images of composite films at various volume ratios. b) i) Open-circuit voltage and ii) short-circuit current density of the sponge-shaped PDMS film with various pore ratios. iii) Relative permittivity changes as a function of pore content. The insets show SEM images of sponge films at various pore ratios. The scale bars are 1 mm. Reproduced with permission.[79] Copyright 2016, ACS.

controlled by a poly(tert-butyl acrylate) (PtBA) grafting ratio. Due to the $\pi$-bonding and polar characteristics of the ester functional groups in the PtBA, the PtBA-grafted PVDF was mainly composed of $\alpha$-phase with increasing dielectric constant, generating twice the enhancement in triboelectric output power compared to a pristine PVDF-based triboelectric devices.

#### *4.2.2. Charge Trap*

To reduce the loss of triboelectric charge and improve the charge storage capability, additional charge trap materials have been introduced into the polymer dielectric (Figure 3f). The first approach was through adding polymer interlayers. This is because the physical defects (amorphous free volume, crosslinking points, or imperfections of crystal lattice) and chemical defects (dangling bonds or functional groups) in polymer materials can act as a charge trap site.[80–82] The preliminary study regarding multi-layered polymer structures was suggested by Cui et al. with the dynamic charge model.[39] By adding polystyrene (PS) "charge storage" layer on the bottom of the PVDF friction layer (or charge transfer layer), the resulting triboelectric devices showed 7-fold improvement of total charge density compared to a single PVDF-based device because most of the triboelectric charge were stored in the PS layer (**Figure 8**a). A three-layered structure was also proposed to further enhance the output performance. To reduce the triboelectric charge attenuation effect during contact electrification by the accumulated charge in the PS layer, a highly conductive carbon nanotubes (CNTs) "charge transport" layer was added between PS and PVDF layer. As a result, this three-layered structure raised the total charge density by a factor of 11.2. The charge storage effect of the multi-layered structure was also reported by Feng et al.[83] After adding a polyimide (PI) charge storage layer under the PVDF friction layer, the triboelectric devices exhibited a 6-fold enhancement of short-circuit current. The role of chemical structures in materials for charge storage capability was also demonstrated. Among three different materials, including PI, PET and cellulose (i.e., paper), PI showed the best device performance as a charge storage layer because non-uniform energy levels along the aromatic rings in the PI chains generate much more trapping sites.[84] Kim et al. demonstrated a triboelectric device with PDMS interlayer.[40] Due to the physical traps in amorphous phase and the crosslinking networks, and chemical traps in the functional groups, the triboelectric device with PDMS interlayer showed 173-fold increased output power density compared to the single-layered device. When compared the charge storage capability to PS, PDMS-PVDF double-layered structure exhibited much higher surface potential than PS-PVDF device because the charge trap density in PDMS is much higher than that in PS. The other approach for charge trapping was the introduction of inorganic materials into the polymer matrix. Wu et al. reported that the 2D materials, such as reduced graphene oxide (rGO) and molybdenum disulfide ($MoS_2$), could suppress the loss of triboelectric charge in the polymer dielectric because the large surface area and quantum confinement effect enabled the charge trapping.[85,86] As a result, the TENG with PI/$MoS_2$/PI structure exhibited 120 times greater power density than that of the device without $MoS_2$ (Figure 8b). A titanium oxide ($TiO_x$)-based electron "blocking" layer was reported by Park et al.[87] The $TiO_x$ film with a thickness of 100 nm was introduced on the dielectric-electrode interface to "block" charge recombination, while other methods have

 © 2021 Wiley-VCH GmbH

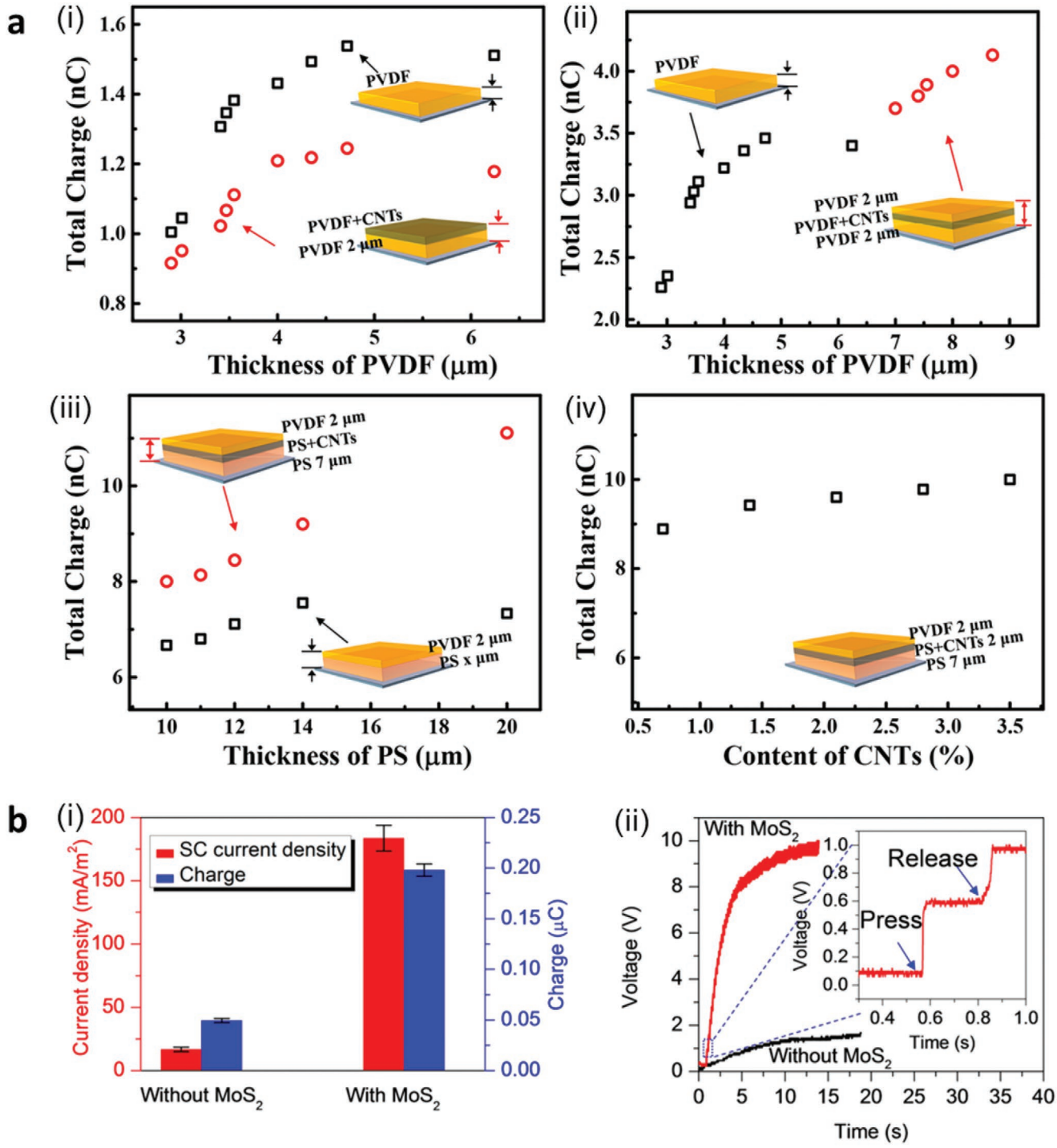


**Figure 8.** a) Measured total surface charge in the dielectric (i.e., friction or contact) layer of triboelectric devices with different structures. b) i) Short-circuit current density (red) and the amount of charge (blue) generated during a contact-separation (i.e., press-release) cycle for the triboelectric devices with and without monolayer $MoS_2$. ii) Charging processes by using the triboelectric devices. The inset is a detailed enlarged view. Reproduced with permission.[39,86] Copyright 2016, 2017, ACS.

focused on "storage" of triboelectric charge by manipulating the dielectric layer. Furthermore, a high permittivity of $TiO_x$ enabled additional polarization of dielectric layer, causing improvement of surface charge density. As a result, due to the coupling effect of electron blocking and enhanced polarization, 25 times greater output power was observed in the TENG with PDMS/$TiO_x$ double-layer relative to that of single-layered PDMS device.


© 2021 Wiley-VCH GmbH

## 5. Summary and Perspectives

As a relatively new alternating energy source, triboelectric devices have been attracting significant attention due to their high performance, high efficiency, low cost, and ease of fabrication. In particular, the diverse choice of materials is a significant advantage of this technology compared to other energy generation methods. Hence, a number of combinations of materials have been suggested depending on the target application and performance level. However, interestingly, most of the materials were selected based on their position on the triboelectric series, despite such tables being arranged empirically, without considering fully the mechanical or chemical properties of the materials. To clarify the operating principles and suggest guidelines for materials selection, theoretical models and strategies to improve device performance have been discussed.

Based on the review, the material-related issues and problems that need to be addressed for further improvement of triboelectric devices are summarized as follows. First of all, understanding the fundamental mechanisms of contact electrification is necessary. Although a few hypotheses of contact electrification have been proposed, no substantial conclusion has been reached.[4] Utilization of advanced scanning probe microscopy techniques would be helpful to investigate the principle of contact electrification. Second, reliable tribo-positive materials should be developed. Although triboelectric devices based on pairs of materials located at the extreme opposite ends of the triboelectric series are expected to show superior energy harvesting capabilities, the majority of the research to date has almost exclusively focused on tribo-negative materials, such as PTFE, PVDF, and PDMS. Furthermore, the vast majority of materials on the positive side of the triboelectric series are biological or natural materials, such as human skin and cotton, and have relatively low mechanical stiffness and/or formability. Therefore, the development of robust tribo-positive materials is crucial not only to improve the performance triboelectric devices but also to extend the range of application. Third, there is a need to investigate mechanically durable functionalized layers. Since triboelectric devices are mechanical contact-based energy generators, abrasion of the contact surface is inevitable. In this respect, despite ion injection being the most effective way to increase the surface charge density, the persistence of the injected charge should be confirmed in advance. In addition, although the surface functionalization method is scientifically meaningful to investigate the contact electrification mechanism, it cannot be applied to practical devices due to the low durability of the functionalized layer. Therefore, advanced functionalization methods and/or functionalized layer with mechanical durability should be developed. Fourth, the development of polymer materials with high-intensity spontaneous polarization would be a good approach to enhance device performance. With respect to durability, control of spontaneous polarisation is the most feasible method among various triboelectric charge generation techniques, as it relies on altered internal molecular structures of the dielectric layer. In this respect, if we can further increase the intensity of spontaneous polarization in conventional ferroelectric polymers, it would also serve to increase the triboelectric device output. However, the required additional electrical poling process with a high electric field for the polymer dielectric layer needs to be addressed. Fifth, the improvement of dynamic charge model is essential. The dynamic charge model has given outstanding insight regarding charge storage and loss phenomena. Thus, it should be extended to the device level, merging with latest device-related models, such as the distance-dependent electric field model and/or the resistance–capacitance product matching model. Sixth, polymer-based nanocomposites have a high potential as a next-generation material for triboelectric devices. The approaches for output performance improvement by tuning the dielectric constant and/or charge trapping can be further investigated through nanocomposite structures. Although several nanocomposite-based TENGs have been suggested already, novel combinations of materials still could be introduced to TENG research. Furthermore, applying the techniques and ideas in the well-established nanocomposite field would be a good approach to enhance TENG performance. Seventh, it is worth investigating the materials with a multilayered structure. Various material combinations for multilayered structures can be investigated for high-performance triboelectric devices. In particular, polymer-based nanocomposites can also be employed as an interlayer. The role of additional layers, including charge storage, charge transfer, and electron blocking layers, need to be studied in more detail. Lastly, environmentally and chemically durable materials should be developed. Since most of the proposed performance enhancement approaches in this review are directly related to the materials, if the operation environment or condition, such as humidity and pH, changes the materials' properties, the performance of the device could deteriorate significantly. Therefore, development of the environmentally and chemically durable materials id crucial to achieve reliable triboelectric device performance.

Since 2012, the performance of triboelectric generators has increased dramatically, and this high performance outplays many existing technologies in its category.[3] Recently, even higher enhancement of the output performance of triboelectric devices has been demonstrated by materials-related approaches. The resultant highly efficient triboelectric generators fabricated by selecting novel materials will enable the realization of sustainable power sources for applications in Internet-of-Things wireless devices and portable/wearable electronics. Furthermore, this approach could enable us to achieve self-powered sensors for pressure, motion, trajectory, vibration, acoustic, chemical, and biomedical applications. Lastly, newly developed materials will increase the viability of triboelectric generators for harvesting large-scale energy from natural sources, such as water, wave and wind energy.

## Acknowledgements

S.K-N. acknowledges support from the European Research Council through an ERC Starting Grant (Grant No. ERC-2014-STG-639526, NANOGEN) and the EPSRC grant "Centre for Advanced Materials for Integrated Energy Systems (CAM-IES)" EP/P007767/1. Y.S.C. is grateful for studentship funding through the Cambridge Commonwealth, European & International Trust.

## Conflict of Interest

The authors declare no conflict of interest.


© 2021 Wiley-VCH GmbH

## Keywords

energy generators, energy harvesting, materials, TENGs, triboelectric

Received: December 8, 2020
Published online: January 14, 2021

[1] S. Katzir, *Arch. Hist. Exact Sci.* **2003**, *57*, 61.
[2] Z. L. Wang, *Adv. Energy Mater.* **2020**, *10*, 2000137.
[3] Z. L. Wang, *ACS Nano* **2013**, *7*, 9533.
[4] Z. L. Wang, J. Chen, L. Lin, *Energy Environ. Sci.* **2015**, *8*, 2250.
[5] R. Hinchet, S.-W. Kim, *ACS Nano* **2015**, *9*, 7742.
[6] B. Chen, Y. Yang, Z. L. Wang, *Adv. Energy Mater.* **2018**, *8*, 1702649.
[7] S. Matsusaka, H. Maruyama, T. Matsuyama, M. Ghadiri, *Chem. Eng. Sci.* **2010**, *65*, 5781.
[8] R. G. Horn, D. T. Smith, *Science* **1992**, *256*, 362.
[9] R. G. Horn, D. T. Smith, A. Grabbe, *Nature* **1993**, *366*, 442.
[10] R. Hinchet, H. Yoon, H. Ryu, M. Kim, E. Choi, *Science* **2019**, *494*, 491.
[11] D. J. Lacks, *Nat. Rev. Chem.* **2019**, *3*, 465.
[12] M. Willatzen, L. C. Lew Yan Voon, Z. L. Wang, *Adv. Funct. Mater.* **2020**, *30*, 1910461.
[13] C. Liu, A. J. Bard, *Nat. Mater.* **2008**, *7*, 505.
[14] B. Baytekin, H. T. Baytekin, B. A. Grzybowski, *J. Am. Chem. Soc.* **2012**, *134*, 7223.
[15] M. Markevitch, W. Forman, C. Jones, M. Donahue, G. M. Voit, D. H. Lumb, G. W. Pratt, U. G. Briel, S. S. Murray, K. Roettiger, M. Ledlow, A. Klypin, L. Rudnick, C. D. Archive, M. States, *Science* **2013**, *341*, 1368.
[16] C. Xu, Y. Zi, A. C. Wang, H. Zou, Y. Dai, X. He, P. Wang, Y.-C. Wang, P. Feng, D. Li, Z. L. Wang, *Adv. Mater.* **2018**, *30*, 1706790.
[17] Z.-L. Wang, A. C. Wang, *Mater. Today* **2019**, *30*, 34.
[18] L. S. McCarty, G. M. Whitesides, *Angew. Chem., Int. Ed.* **2008**, *47*, 2188.
[19] H. T. Baytekin, A. Z. Patashinski, M. Branicki, B. Baytekin, S. Soh, B. A. Grzybowski, *Science* **2011**, *333*, 308.
[20] C. A. Mizzi, A. Y. W. Lin, L. D. Marks, *Phys. Rev. Lett.* **2019**, *123*, 116103.
[21] S. Lin, L. Xu, C. Xu, X. Chen, A. C. Wang, B. Zhang, P. Lin, Y. Yang, H. Zhao, Z. L. Wang, *Adv. Mater.* **2019**, *31*, 1808197.
[22] J. F. Kok, D. J. Lacks, *Phys. Rev. E* **2009**, *79*, 51304.
[23] J. Henniker, *Nature* **1962**, *196*, 474.
[24] H. Zou, Y. Zhang, L. Guo, P. Wang, X. He, G. Dai, H. Zheng, C. Chen, A. C. Wang, C. Xu, Z. L. Wang, *Nat. Commun.* **2019**, *10*, 1427.
[25] S. Niu, S. Wang, L. Lin, Y. Liu, Y. S. Zhou, Y. Hu, Z. L. Wang, *Energy Environ. Sci.* **2013**, *6*, 3576.
[26] S. Wang, L. Lin, Y. Xie, Q. Jing, S. Niu, Z. L. Wang, *Nano Lett.* **2013**, *13*, 2226.
[27] S. Niu, Y. Liu, S. Wang, L. Lin, Y. S. Zhou, Y. Hu, Z. L. Wang, *Adv. Funct. Mater.* **2014**, *24*, 3332.
[28] S. Niu, Y. Liu, X. Chen, S. Wang, Y. Sheng, L. Lin, Y. Xie, Z. Lin, *Nano Energy* **2015**, *12*, 760.
[29] G. Zhu, J. Chen, T. Zhang, Q. Jing, Z. L. Wang, *Nat. Commun.* **2014**, *5*, 3426.
[30] Y. Yang, G. Zhu, H. Zhang, J. Chen, X. Zhong, Z.-H. Lin, Y. Su, P. Bai, X. Wen, Z. L. Wang, *ACS Nano* **2013**, *7*, 9461.
[31] H. Zhang, Y. Yang, X. Zhong, Y. Su, Y. Zhou, C. Hu, Z. L. Wang, *ACS Nano* **2014**, *8*, 680.
[32] Y. Yang, H. Zhang, Z.-H. Lin, Y. S. Zhou, Q. Jing, Y. Su, J. Yang, J. Chen, C. Hu, Z. L. Wang, *ACS Nano* **2013**, *7*, 9213.
[33] Q. Jing, Y. S. Choi, M. Smith, N. C´atic´, C. Ou, S. Kar-Narayan, N. Ćatić, C. Ou, S. Kar-Narayan, *Adv. Mater. Technol.* **2019**, *4*, 1900048.
[34] L. Lin, Y. Xie, S. Niu, S. Wang, P.-K. Yang, Z. L. Wang, *ACS Nano* **2015**, *9*, 922.
[35] Y. Zi, S. Niu, J. Wang, Z. Wen, W. Tang, Z. L. Wang, *Nat. Commun.* **2015**, *6*, 8376.
[36] R. D. I. G. Dharmasena, K. D. G. I. Jayawardena, C. A. Mills, J. H. B. Deane, J. V. Anguita, R. A. Dorey, S. R. P. Silva, *Energy Environ. Sci.* **2017**, *10*, 1801.
[37] R. D. I. G. Dharmasena, K. D. G. I. Jayawardena, C. A. Mills, R. A. Dorey, S. R. P. Silva, *Nano Energy* **2018**, *48*, 391.
[38] J. Peng, S. D. Kang, G. J. Snyder, *Sci. Adv.* **2017**, *3*, eaap8576.
[39] N. Cui, L. Gu, Y. Lei, J. Liu, Y. Qin, X. Ma, Y. Hao, Z. L. Wang, *ACS Nano* **2016**, *10*, 6131.
[40] D. W. Kim, J. H. Lee, I. You, J. K. Kim, U. Jeong, *Nano Energy* **2018**, *50*, 192.
[41] P. Bai, G. Zhu, Z.-H. Lin, Q. Jing, J. Chen, G. Zhang, J. Ma, Z. L. Wang, *ACS Nano* **2013**, *7*, 3713.
[42] X.-S. Zhang, M.-D. Han, R.-X. Wang, F.-Y. Zhu, Z.-H. Li, W. Wang, H.-X. Zhang, *Nano Lett.* **2013**, *13*, 1168.
[43] Q. Jing, S. Kar-Narayan, *J. Phys. D: Appl. Phys.* **2018**, *51*, 303001.
[44] F. R. Fan, L. Lin, G. Zhu, W. Wu, R. Zhang, Z. L. Wang, *Nano Lett.* **2012**, *12*, 3109.
[45] S. Wang, L. Lin, Z. L. Wang, *Nano Lett.* **2012**, *12*, 6339.
[46] G. Zhu, C. Pan, W. Guo, C. Y. Chen, Y. Zhou, R. Yu, Z. L. Wang, *Nano Lett.* **2012**, *12*, 4960.
[47] C. K. Jeong, K. M. Baek, S. Niu, T. W. Nam, Y. H. Hur, D. Y. Park, G. Hwang, M. Byun, Z. L. Wang, Y. S. Jung, K. J. Lee, *Nano Lett.* **2014**, *14*, 7031.
[48] S. S. Kim, J. H. Lee, R. Hinchet, K. Kim, S. Kim, *Energy Environ. Sci.* **2015**, *8*, 3605
[49] K. Y. Lee, H. J. Yoon, T. Jiang, X. Wen, W. Seung, S. W. Kim, Z. L. Wang, *Adv. Energy Mater.* **2016**, *6*, 1502566.
[50] S. Wang, Y. Xie, S. Niu, L. Lin, C. Liu, Y. S. Zhou, Z. L. Wang, *Adv. Mater.* **2014**, *26*, 6720.
[51] L. Cheng, Q. Xu, Y. Zheng, X. Jia, Y. Qin, *Nat. Commun.* **2018**, *9*, 3773.
[52] J. Wang, C. Wu, Y. Dai, Z. Zhao, A. Wang, T. Zhang, Z. L. Wang, *Nat. Commun.* **2017**, *8*, 88.
[53] W. Liu, Z. L. Z. Wang, G. Wang, G. Liu, J. Chen, X. Pu, Y. Xi, X. Wang, H. Guo, C. Hu, Z. L. Z. Wang, *Nat. Commun.* **2019**, *10*, 1426.
[54] S. Shin, Y. H. Kwon, Y. Kim, J. Jung, M. H. Lee, J. Nah, *ACS Nano* **2015**, *9*, 4621.
[55] G. Song, Y. Kim, S. Yu, M.-O. Kim, S.-H. Park, S. M. Cho, D. B. Velusamy, S. H. Cho, K. L. Kim, J. Kim, E. Kim, C. Park, *Chem. Mater.* **2015**, *27*, 4749.
[56] S. H. Shin, Y. E. Bae, H. K. Moon, J. Kim, S. H. Choi, Y. Kim, H. J. Yoon, M. H. Lee, J. Nah, *ACS Nano* **2017**, *11*, 6131.
[57] Y. Feng, Y. Zheng, S. Ma, D. Wang, *Nano Energy* **2016**, *19*, 48.
[58] Y. H. Kwon, S.-H. Shin, J.-Y. Jung, J. Nah, *Nanotechnology* **2016**, *27*, 205401.
[59] Y. Yu, Z. Li, Y. Wang, S. Gong, X. Wang, *Adv. Mater.* **2015**, *27*, 4938.
[60] H. Ryu, J. H. Lee, T. Y. Kim, U. Khan, J. H. Lee, S. S. Kwak, H. J. Yoon, S. W. Kim, *Adv. Energy Mater.* **2017**, *7*, 1700289.
[61] Y. S. Choi, J. Sung, S. J. Kang, S. H. Cho, I. Hwang, S. K. Hwang, J. Huh, H.-C. Kim, S. Bauer, C. Park, *Adv. Funct. Mater.* **2013**, *23*, 1120.
[62] P. Bai, G. Zhu, Y. S. Zhou, S. Wang, J. Ma, G. Zhang, Z. L. Wang, *Nano Res.* **2014**, *7*, 990.
[63] J.-H. Lee, R. Hinchet, T. Y. Kim, H. Ryu, W. Seung, H.-J. Yoon, S.-W. Kim, *Adv. Mater.* **2015**, *27*, 5553.
[64] K. Y. Lee, S. K. S.-W. Kim, J. Lee, D. Seol, M. K. Gupta, Y. Kim, S. K. S.-W. Kim, *Adv. Funct. Mater.* **2016**, *26*, 3067.
[65] W. Seung, H.-J. Yoon, T. Y. Kim, H. Ryu, J. Kim, J.-H. Lee, J. H. Lee, S. Kim, Y. K. Park, Y. J. Park, S.-W. Kim, *Adv. Energy Mater.* **2017**, *7*, 1600988.
[66] Y. S. Choi, S. K. Kim, M. Smith, F. Williams, M. E. Vickers, J. A. Elliott, S. K. Narayan, *Sci. Adv.* **2020**, *6*, eaay5065.
[67] Y. S. Choi, Q. Jing, A. Datta, C. Boughey, S. Kar-Narayan, *Energy Environ. Sci.* **2017**, *10*, 2180.
[68] Y. S. Choi, S. K. Kim, F. Williams, Y. Calahorra, J. A. Elliott, S. Kar-Narayan, S. K. Kim, F. Williams, Y. Calahorra, S. Kar-Narayan, *Chem. Commun.* **2018**, *54*, 6863.

 © 2021 Wiley-VCH GmbH

[69] Y. S. Choi, S. Kar-Narayan, *EcoMat.* **2020**, *2*, e12063.
[70] T. Busolo, D. P. Ura, S. K. Kim, M. M. Marzec, A. Bernasik, U. Stachewicz, S. Kar-Narayan, *Nano Energy* **2019**, *57*, 500.
[71] J. W. Lee, H. J. Cho, J. Chun, K. N. Kim, S. Kim, C. W. Ahn, I. W. Kim, J. Y. Kim, S. W. Kim, C. Yang, J. M. Baik, *Sci. Adv.* **2017**, *3*, e1602902.
[72] Y. J. Kim, J. Lee, S. Park, C. Park, C. Park, H.-J. Choi, *RSC Adv.* **2017**, *7*, 49368.
[73] Y. Yang, H. Zhang, J. Chen, S. Lee, T. C. Hou, Z. L. Wang, *Energy Environ. Sci.* **2013**, *6*, 1744.
[74] G. Q. Gu, C. B. Han, J. J. Tian, C. X. Lu, C. He, T. Jiang, Z. Li, Z. L. Wang, *ACS Appl. Mater. Interfaces* **2017**, *9*, 11882.
[75] X. He, H. Guo, X. Yue, J. Gao, Y. Xi, C. Hu, *Nanoscale* **2015**, *7*, 1896.
[76] V. K. T. Prateek, R. K. Gupta, *Chem. Rev.* **2016**, *116*, 4260.
[77] Z.-M. Dang, J.-K. Yuan, S.-H. Yao, R.-J. Liao, *Adv. Mater.* **2013**, *25*, 6334.
[78] J. Chun, J. W. Kim, W. Jung, C.-Y. Kang, S.-W. Kim, Z. L. Wang, J. M. Baik, *Energy Environ. Sci.* **2015**, *8*, 3006.
[79] J. Chen, H. Guo, X. He, G. Liu, Y. Xi, H. Shi, C. Hu, *ACS Appl. Mater. Interfaces* **2016**, *8*, 736.
[80] W. W. Shen, H. B. Mu, G. J. Zhang, J. B. Deng, D. M. Tu, *J. Appl. Phys.* **2013**, *113*, 083706.
[81] G. Chen, Z. Xu, *J. Appl. Phys.* **2009**, *106*, 123707.
[82] J. Li, F. Zhou, D. Min, S. Li, R. Xia, *IEEE Trans. Dielectr. Electr. Insul.* **2015**, *22*, 1723.
[83] Y. Feng, Y. Zheng, G. Zhang, D. Wang, F. Zhou, W. Liu, *Nano Energy* **2017**, *38*, 467.
[84] T. Takada, H. Kikuchi, H. Miyake, Y. Tanaka, M. Yoshida, *IEEE Trans. Dielectr. Electr. Insul.* **2014**, *22*, 1240.
[85] C. Wu, T. W. Kim, H. Y. Choi, *Nano Energy* **2017**, *32*, 542.
[86] C. Wu, T. W. Kim, J. H. Park, H. An, J. Shao, X. Chen, Z. L. Wang, *ACS Nano* **2017**, *11*, 8356.
[87] H. W. Park, N. D. Huynh, W. Kim, C. Lee, Y. Nam, S. Lee, K. B. Chung, D. Choi, *Nano Energy* **2018**, *50*, 9.

**Yeonsik Choi** is a postdoctoral researcher in the Department of Materials Science and Engineering and Querrey Simpson Institute for Bioelectronics at Northwestern University, USA. He obtained his B.S. degree in 2009, and his MS degree in 2011 from Yonsei University, S. Korea, in Materials Science and Engineering. He received his Ph.D. degree in 2019 in Materials Science from the University of Cambridge, UK, with support from the Cambridge Trust Scholarship. He was a senior researcher from 2011 to 2015 with the Advanced Materials Development Team at LG Chem. Ltd., S. Korea.

**Sang-Woo Kim** is an SKKU distinguished professor (SKKU Fellow) at Sungkyunkwan University (SKKU). His recent research interest is focused on piezoelectric/triboelectric nanogenerators, self-powered sensors and body-implantable devices, and 2D materials. Prof. Kim is a Director of the BK21 FOUR SKKU MSE Program.

**Sohini Kar-Narayan** is a Reader (associate professor) of Device & Energy Materials at the Department of Materials Science at the University of Cambridge. She received a B.Sc. (Honours) in Physics in 2001 from the University of Calcutta, India, followed by MS (2004) and Ph.D. (2009) in Physics from the Indian Institute of Science, Bangalore. Following a postdoctoral appointment at the Department of Materials Science in Cambridge, she was awarded a prestigious Royal Society Dorothy Hodgkin Fellowship in 2012, and a European Research Council Starting Grant in 2015. Her research focuses on functional nanomaterials for applications in energy, sensing, and biomedicine.


© 2021 Wiley-VCH GmbH